Temperature Transients in a Cylindrical Pressure Vessel Filled from Vacuum

David R. Dowling* and Victor R. Buonadonna†
Boeing Aerospace and Electronics, Seattle, Washington 98124
and
Robert E. Breidenthal‡
University of Washington, Seattle, Washington 98195

The spatially averaged temperature of the gas inside a cylindrical pressure vessel during the time that it is being filled from vacuum has been predicted theoretically and investigated experimentally. The theory, which yields analytic formulas, is based on a heat-transfer model developed from physical and dimensional reasoning. It includes corrections for slow changes in the injection gas reservoir conditions and vessel wall temperature. When the flow is fully turbulent throughout the vessel, the theory predicts that the spatially averaged temperature should be independent of the mass injection rate, and proportional to the inverse one-half power of time. When the heat transfer from the gas to the wall of the pressure vessel occurs across a forced laminar boundary layer, the theory predicts that the spatially averaged temperature should be proportional to the square root of the mass injection rate, and the inverse one-quarter power of time. Experiments performed in a 2.1-m-diam pressure vessel at Reynolds numbers approaching 10^6 agree with the theory in each regime. Measured deviations near Reynolds number 3×10^5 are attributed to boundary-layer transition.

Nomenclature

A_o = injection orifice area
a = speed of sound in the injected gas
c_1, c_2 = dimensionless constants determined from the experiments
c_v = specific heat capacity of the gas at constant volume
c_p = specific heat capacity of the gas at constant pressure
D = diameter of the pressure vessel
E = total internal energy
g = acceleration of gravity
J = thrust per unit length
J_s = thrust from a single injection orifice
M = total mass
$\dot{m}$ = mass flow rate per unit length
$\dot{m}_s$ = mass flow rate from a single injection orifice
N = Nusselt number
P, p = pressure
P_t = pressure inside the cylindrical vessel
P_r = Prandtl number $= \mu c_p/\kappa$
Q_w = heat transferred to the cavity walls per unit time and unit length
R = gas constant, $c_p - c_v$
Re = Reynolds number
S = specific heat capacity of the vessel wall material
T = temperature
t = time
t_a = characteristic acoustic time in the pressure vessel $= \gamma D/a^*(\gamma + 1)$
t_c = characteristic rotation time of a large vortex
t_m = thermal time scale of the pressure vessel
U = mean convection velocity at the edge of a large vortex
V = volume
$\dot{V}$ = volume injection rate of gas per unit length at P_i and T_o
α = $c_1 (\gamma/P_r)$
β = $(\gamma T_o^o/T_w^o) - 1$
χ = $(\gamma t_a/T_w^o)(\Delta T_o/t_f) - 2(t_a/t_m)$
δ = $[P_f t_a/(\gamma + 1)P^* t_f]$
δ_M = momentum boundary-layer thickness
δ_T = thermal boundary-layer thickness
ϕ = $c_2(\gamma/Pr)\sqrt{\mu/\dot{m}}$
γ = ratio of specific heats (c_p/c_v)
κ = thermal conductivity of the gas
μ = absolute viscosity of the gas
θ = dimensionless temperature difference $= (T_g - T_w)/T_w^o$
ρ = gas density
τ = dimensionless time (t/t_a)
τ_w = wall shear stress
ν = kinematic viscosity of the gas $= \mu/\rho$

Superscripts

f = final
o = original, initial
$*$ = sonic condition

Subscripts

f = final
g = gas
i = injection
o = reservoir
w = wall

Introduction

THE use of vacuum and pressure vessels is exceedingly common in aerospace engineering. The size range of useful devices is enormous. For example, the large vacuum chambers that are used to test full-scale spacecraft have diameters greater than 10 m, while the small propellant tanks that are used in the attitude-adjustment systems of satellites and space probes can be as small as a few centimeters in diameter. Somewhere in between these sizes are the specialized pressure vessels used to contain the active medium gases of pulsed lasers. In most cases, at least one step in the gas flow cycle of a pulsed laser involves filling the laser vessel from vacuum.

Compressive heating of the gas inside the laser cavity from the work done during the injection process causes the gas

Received May 8, 1989; revision received Oct. 23, 1989.

*Currently, Postdoctoral Scientist, Applied Physics Laboratory, University of Washington. Member AIAA.
†Senior Research Engineer.
‡Professor, Department of Aeronautics and Astronautics, Consultant to Boeing Aerospace and Electronics. Member AIAA.

temperature to rise. This energy is eventually transferred to the walls of the laser cavity by the resulting motion of the gas and by thermal conduction. Turbulence generated by the injection system during the fill from vacuum leads to thermal fluctuations in the gas until the cavity walls and the gas equilibrate. Temperature fluctuations (i.e., index of refraction fluctuations) in the active medium gas at the time that the laser is fired degrade the quality of the beam that the laser produces.[1] In many turbulent flows, the rms (root-mean-square) fluctuation of a convected scalar-like temperature is a constant percentage of the mean temperature deviation. Hence, quantifying the mean temperature difference between the gas and the walls of the laser cavity is an important first step toward understanding and possibly minimizing temperature fluctuations in the gas.

This paper describes a theoretical and experimental effort to understand the temporal evolution of the spatially averaged temperature inside a pressure vessel as it is filled from vacuum at a constant rate. Yang[2] and Kato[3] developed formulas for the time for venting or charging a pressurized volume, but they did not directly address changes in gas temperature or explicitly incorporate heat transfer to the cavity walls. The theory presented in the next section accounts for gas-wall heat transfer as well as slow changes in the injected gas reservoir temperature and vessel wall temperature. The predictions of the current theory compare favorably with temperature measurements made in a 2.1-m-diam cylindrical pressure vessel at Reynolds numbers up to 6×10^5. The experimental technique is described in the third section of this paper. The experimental results, a short discussion, and the conclusions comprise the final three sections.

Although this research was driven by the needs of the pulse laser community, the theoretical approach presented below may be general enough to be applied, perhaps with small modifications for vessel geometry, to many situations in aerospace, mechanical, and chemical engineering where the gas temperature inside a pressure vessel is important.

Theory

When gas is injected into a volume initially evacuated, adiabatic compressive heating effects will cause the gas temperature to rise. For a calorically perfect gas without heat transfer to the walls of the vessel, the temperature of the gas should be independent of the vessel pressure and equal to γT_o (see Appendix). This result requires that the temperature of the gas rise significantly on injection (almost 120°C for air with T_o near room temperature). Such a large temperature rise does not occur in practice because of heat transfer from the gas to the walls of the pressure vessel.

While the vessel is being pressurized, the Reynolds and Mach numbers of the flow inside the vessel vary from nearly zero and supersonic, respectively, at the beginning, to final values that can be large (of order 10^5 in the current experiments) and nearly zero, respectively. It was not possible theoretically to treat the entire range of both parameters; so, to make the formulation of the problem realistic, and yet still tractable, several assumptions were made. These are presented and discussed in the following list.

1) The pressure vessel is a long cylinder of length L and diameter D, with L much greater than D. This shape makes it possible to ignore the effect of the vessel's end caps and is also of great interest for the pulsed laser application.

2) The gas injection system is a single row of closely spaced injection orifices (see Fig. 1). This injection geometry was considered because its mixing capability has been characterized,[4] and it quickly establishes two-dimensional flow in the plane perpendicular to the cylindrical axis.

3) The mass injection rate is determined by sonic flow through fixed-size orifices. As long as the orifices are choked, the mass flux through them depends only on the reservoir conditions and is independent of the downstream pressure. In all but the longest experimental run, the orifices remained choked and the mass flux varied by less than 1 or 2%.

4) The Mach number of the recirculating flow inside the vessel is much less than one. This assumption is not justified at the beginning of the fill when regions of supersonic flow fill a significant part of the vessel's interior. However, as the vessel pressure increases, the supersonic regions decrease in size and should have little effect on the heat transfer to the vessel walls as long as $P_t D^2 / P_i A_o > 10^3$ or so (this criterion places the Mach disk in the supersonic injection stream less than 0.03 D from the orifice).[5] For all of the experiments discussed in the next section, this parameter was above 10^3 for the final 80-90% of the fill.

5) The rate of change of the reservoir gas temperature and pressure due to imperfections in the delivery system is small compared to the rate of change of the vessel gas temperature and pressure. This assumption allows some of the imperfections in the experimental setup to be included in a simple way in the theoretical framework. For example, T_o typically dropped by a few degrees Kelvin during an experiment due to isentropic expansion in the finite-size injection gas reservoir, and Joule-Thompson cooling in the delivery plumbing.

6) The thermal mass of the pressure vessel is finite but much larger than the thermal mass of the injected gas. For the current experimental setup, $SM_w / c_v M_g \approx 200$.

7) The wall of the pressure vessel is thermally thin (i.e., uniform in temperature throughout its thickness).

8) The outer surface of the pressure vessel is adiabatic (perfectly insulated). Assumptions 6, 7, and 8 are useful in simplifying the prediction of the vessel wall temperature during the gas fill process.

9) The injected gas is calorically perfect over the range of interest once it reaches the interior of the pressure vessel. This assumption was included to simplify the analysis; it could be removed by resorting to numerical solution techniques. It is justified in this study by the relatively low pressures ($< 10^5$ Pa) and moderate temperatures (≈ 300 K) of the gas inside the pressure vessel. An adjustment for real-gas effects that took place in the gas delivery system was made in processing the experimental data.

10) Buoyancy forces are unimportant. This assumption allows fluid momentum to be conserved independently of the fluid energy. It is justified in this study by the fact that an estimate of the global Richardson number ($\theta g D / U^2$) for the recirculating flow inside the experimental vessel was less than unity for all but the longest run.

11) Temperature variations are not large enough to cause significant changes in the transport coefficients of the gas. This assumption simplifies the analysis. It could be eliminated through the use of numerical solution techniques.

The starting point for this analysis is the integral form of the energy conservation equation for a flowing fluid (for example, see Thompson[6]). Based on the symmetry produced by assumptions 1 and 2, consider a control volume that encloses a slice of gas inside the pressure vessel and perform a spatial integration in the plane perpendicular to the cylindrical axis. Assumption 4 allows the kinetic energy terms to be dropped. The simplified energy equation can then be written:

$$\frac{\mathrm{d}(c_v \dot{m} t T_g)}{\mathrm{d}t} = -Q_w + \dot{m} c_v T_o + P_i \dot{V}_i \qquad (1)$$

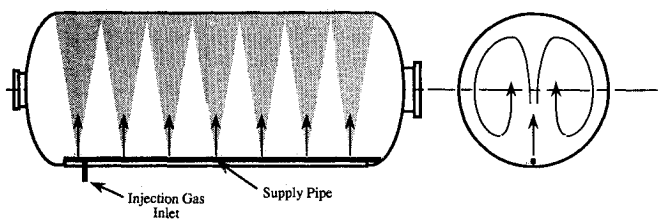

Fig. 1. The gas injection system.

The extensive variables in this equation are per-unit-length quantities, and T_g represents a spatial average of the gas temperature in a cross section of the cylindrical pressure vessel. The term on the left-hand side of Eq. (1) is the time rate of change of the energy of the gas inside the pressure vessel. The three terms on the right-hand side of the equation are, from left to right, the heat transferred to the walls of the vessel, the energy carried into the pressure vessel by the injected gas, and the work done on the gas in the pressure vessel by the injected gas. Assumptions 5 and 9 allow the time derivative of the perfect gas law, $PV = mRT$, to be used to change the final term on the right-hand side to $\dot{m}RT_o$ which can then be combined with the second term on the right-hand side, using the definition of R to yield $\dot{m}c_pT_o$.

The heat transfer term can be expressed in terms of the Nusselt number

$$Q_w = N\kappa(T_g - T_w) \tag{2}$$

where T_w should not be treated as constant (assumption 6). However, assumption 6 does suggest that the walls of the pressure vessel can be treated like a very low-pass filter to thermal fluctuations in the gas. This notion, plus the fact that the rate of work input is essentially constant, and assumption 8 imply that including the linear term from a Taylor series expansion of T_w in powers of t should be an accurate correction to simply taking $T_w = T_w^o$.

The magnitude of the linear correction term can be estimated from a global energy balance of both the injected gas and the pressure vessel, given that the approximate final state of the combined gas/vessel system is isothermal (assumptions 6 and 7). The total initial energy of the whole system is $(c_vM_gT_o + SM_wT_w^o)$. The total work input is $P_iV_i(=M_gRT_o)$. The final energy is $(c_vM_g + SM_w)F_w^f$. Balancing these yields

$$(c_v + R)M_gT_o + SM_wT_w^o = (c_vM_g + SM_w)T_w^f \tag{3}$$

When Eq. (3) is solved for T_w^f, and the total wall temperature change for the whole fill, $\Delta T_w = T_w^f - T_w^o$, is computed, the linearly corrected expression for T_w becomes

$$T_w = T_w^o + \frac{t}{t_f}(\Delta T_w) = T_w^o\left(1 + \frac{t}{t_m}\right)$$

where

$$t_m^{-1} = \frac{(c_pT_o - c_vT_w^o)\dot{m}}{M_wST_w^o} \tag{4}$$

and M_g/t_f is equal to $\dot{m}$. t_m is a time constant associated with the total heat capacity of the pressure vessel. It is expected that small variations in T_o (up to a few percent of the initial T_o) during the fill will not produce large enough changes in t_m to affect the final results for T_g. In the experiments, ΔT_w was typically about 1°C.

If Eq. (1) is divided by $T_w^oc_v\dot{m}$, and a dimensionless temperature difference, $\theta = (T_g - T_w)/T_w^o$, is introduced to replace T_g, the result is

$$\frac{d(t\{\theta + t/t_m\})}{dt} = -\frac{N\kappa\theta}{\dot{m}c_v} + \left(\gamma\frac{T_o}{T_w^o} - 1\right) \tag{5}$$

where T_o can be a slowly varying function of time, and assumptions 3 and 5 have been used to remove $\dot{m}$ from the time derivative. It should be noted that the normalization of T_g chosen to produce θ is the one relevant for laser performance since the gas that is inside the vessel only "knows about" the temperature of wall that it contacts and the rate that work is being done on it. Equation (5) is a first-order, linear equation in θ provided N is only a function of time and does not depend on θ. This condition is satisfied as long as assumptions 10 and 11 are true, so that the solution of Eq. (5) can be carried out if a relation for $N(t)$ can be found.

To find a relation for $N(t)$, it is necessary to consider the mechanism of heat transport. The relevant formulation (without radiative heat transfer) for Q_w is given by

$$Q_w = -\pi D\kappa\langle(\partial T/\partial n)|_{(\text{at the wall})}\rangle \tag{6}$$

where the $\langle\ \rangle$ brackets denote a spatial average, and n is a coordinate that is perpendicular to the wall. The mean temperature derivative in Eq. (6) can be replaced by the mean temperature difference $\Delta T = T_g - T_w$ and an effective thermal boundary-layer thickness

$$Q_w = -\pi D\kappa\Delta T/\delta_T \tag{7}$$

Making use of Reynolds' analogy,[7,8] the assumption that heat and momentum are transferred by similar processes, δ_T can be estimated from considerations of the mean momentum transfer.

Previous work[4] has shown that the mean motion inside the pressure vessel for this injection system will consist of two large counter-rotating vortices (see the cross-sectional illustration in Fig. 1). The time for the rotation of these vortices was found to be proportional to a characteristic time t_c produced from dimensional considerations of the relevant parameters:

$$t_c^2 = \frac{\rho D^3}{J} \tag{8}$$

It was also shown that the characteristic velocity scale of the flowfield is given by D/t_c. The large vortices will be turbulent since they are produced by the impingement of fully developed axisymmetric turbulent jets on the vessel wall, and they constitute the largest scale of a high-Reynolds-number (of order 10^5 in the current experiments) shear flow.

The mean gas motion in the vessel will be driven by the thrust of the injection jets. The rotation of the large vortices will be impeded by the skin friction and the pressure distribution on the vessel walls. In particular, the impact zone on the opposite wall from the injection jets will be at a slightly higher pressure Δp when compared to other parts of the vessel interior. The circumferential length of the portion of the wall where the over pressure is significant will be proportional to the diameter of the vessel. For a quasisteady state, the three forces will balance, which means that

$$J \approx \pi D\tau_w + fD\Delta p \tag{9}$$

where f is a dimensionless constant of order unity. The over pressure Δp will be proportional to the dynamic pressure of the flow at the edges of the vortices. The boundary layer on the vessel wall may be turbulent, laminar, or in transition.

Consider first the flow regime with a turbulent boundary layer. Both Δp and τ_w will have the same functional dependence on the bulk flow:

$$\Delta p \text{ and } \tau_w \propto \rho U^2 \tag{10}$$

Using the momentum transfer equivalent of Eqs. (6) and (7), τ_w can be expressed as

$$\tau_w = \mu\langle(\partial u/\partial n)|_{(\text{at the wall})}\rangle = \mu U/\delta_M \tag{11}$$

The f and the skin-friction coefficient should be independent of the Reynolds number at high Reynolds number. This concept can be combined with Eqs. (8–11) and the Reynolds analogy, i.e., $\delta_T \approx \delta_M$, to yield the functional dependence of the boundary-layer thicknesses. The result, ignoring dimensionless constants, is

$$\delta_T \approx \delta_M \propto \mu(D/\rho J)^{1/2} = \nu t_c/D \tag{12}$$

This thickness physically corresponds to the laminar sublayer thickness of a turbulent boundary layer. Combining Eqs. (2),

(7), (9), (10), and (12) yields

$$N \propto \frac{UD}{\nu} = Re \equiv \frac{(\rho JD)^{1/2}}{\mu} \tag{13}$$

The dependence of N on Re displayed in Eq. (13) is typical for turbulent heat transfer.[8] The gas density ρ is proportional to $\dot{m}t/D^2$, while D and μ are constant throughout the fill process (assumption 11). The thrust J should be nearly constant but may decrease by a few percent because of the changing back pressure inside the pressure vessel [see Eq. (17)]. Therefore, without small corrections for variation of J,

$$N \text{ and } Re \propto t^{1/2} \tag{14}$$

The governing equation can now be rewritten with the basic time dependence of the heat-transfer term shown explicitly:

$$\frac{d(t\{\theta + t/t_m\})}{dt} = -c_1 \frac{\gamma\theta}{Pr}\sqrt{\frac{Jt}{\dot{m}D}} + \left(\gamma \frac{T_o(t)}{T_w^o} - 1\right) \tag{15}$$

where $\dot{m}D/J$ is the natural time scale of the problem. For sonic injection orifices (assumption 3), then $\dot{m}D/J$ is given by

$$\frac{\dot{m}D}{J} = \frac{\rho^* a^* A_o D}{\rho^* a^{*2} A_o + (P^* - P_t)A_o} \tag{16}$$

This can be further simplified by using the perfect gas law at sonic conditions, and the perfect gas relation for $a^*, a^* = \sqrt{\gamma R T^*}$, where $T^* = 2T_o/(\gamma + 1)$:

$$\frac{\dot{m}D}{J} = \frac{D}{a^*\left[1 + \frac{1}{\gamma}\left(1 - \frac{P_t}{P^*}\right)\right]} \tag{17}$$

Since the vessel pressure rises during a run, J is not strictly constant but instead depends slightly on time. In the same spirit as the correction for T_w, only the linear term in the Taylor series expansion of P_t will be kept. The magnitude of the correction can be estimated from the final vessel pressure. These manipulations yield

$$P_t = P_f \frac{t}{t_f} \tag{18}$$

and

$$\frac{\dot{m}D}{J} = \frac{D}{a^*\left[1 + \frac{1}{\gamma}\left(1 - \frac{P_f}{P^*}\frac{t}{t_f}\right)\right]} \tag{19}$$

If $P^* \gg P_f$, which was true for most of the experiments, then $\dot{m}D/J$ is essentially a constant t_a, which is an acoustic time scale for the vessel.

$$t_a = \frac{\gamma D}{a^*(\gamma + 1)} \tag{20}$$

It is worth noting that Eq. (16) is accurate for P_t above and below P^* as long as the first-order difference, $|P_t - P|/P^*$, is small compared to unity. For argon, the gas used in the experiments, P^* is about 49% of P_i.

Combining Eqs. (15), (19), and (20) yields the rate equation for the first flow regime:

$$\frac{d(t\{\theta + t/t_m\})}{dt} = -c_1 \frac{\gamma\theta}{Pr}\left[\frac{t}{t_a}\left(1 - \frac{P_f t}{(\gamma + 1)P^* t_f}\right)\right]^{1/2} + \left(\gamma \frac{T_o(t)}{T_w^o} - 1\right) \tag{21}$$

The approximations leading to Eq. (21) are consistent with fully turbulent flow throughout the pressure vessel. Hence, the solutions of Eq. (21) cannot be correct when the Reynolds number is small, such as at the beginning of the fill. Note that in the limit of $P^* \gg P_f$ and $t_m \to \infty$, Eq. (21) does not contain the mass flow rate so the solution for θ in this regime will be independent of $\dot{m}$.

The second flow regime to be considered is different from the first in that the turbulent flow in the central region of the pressure vessel interacts with the vessel wall through a forced laminar boundary layer and not a turbulent one. Because of this difference, the formulation of the Nusselt number is based on an effective boundary-layer thickness derived from the forcing parameters of the large vortices

$$\delta_T \propto \sqrt{\nu D/U} \tag{22}$$

Since the skin-friction coefficient is usually much smaller than unity, the pressure term in Eq. (9) must dominate the force balance, i.e.,

$$J \propto \rho U^2 D \tag{23}$$

These two relations are consistent with fully turbulent flow everywhere inside the vessel except for a forced laminar boundary layer on the inside wall. In this case, Eqs. (2), (5), (7), (19), (20), (22), and (23) can be used to obtain $\delta_T \propto (\nu t_c)^{1/2}$, the typical Nusselt number dependence for laminar heat transfer[8]; i.e., $N \propto (Re)^{1/2}$, and

$$\frac{d(t\{\theta + t/t_m\})}{dt} = -c_2 \frac{\gamma\theta}{Pr}\sqrt[4]{\frac{\mu^2}{\dot{m}^2}\frac{t}{t_a}\left(1 - \frac{P_f t}{(\gamma + 1)P^* t_f}\right)} + \left(\gamma \frac{T_o(t)}{T_w^o} - 1\right) \tag{24}$$

Note that this equation explicitly contains $\dot{m}$, so that the solutions for θ at different $\dot{m}$ will not fall on a single curve.

A theoretical treatment of the boundary-layer transition regime was not attempted.

Both Eqs. (21) and (24) are of the form

$$\frac{d(\tau\theta)}{d\tau} = -\alpha\theta\tau^{\epsilon}(1 - \delta\tau)^{\epsilon} + \varphi(\tau) \tag{25}$$

where α and δ are dimensionless constants and $\tau = t/t_a$. The exact particular solution with $\tau \cdot \theta(\tau) = 0$ at $\tau = 0$ is given by

$$\theta = \frac{\exp\{-\int_0^\tau \alpha(1 - \delta\zeta)^{\epsilon}\zeta^{\epsilon - 1}\, d\zeta\}}{\tau} \times \int_0^\tau \varphi(\xi) \exp\{+\int_0^\xi \alpha(1 - \delta\zeta)^{\epsilon}\zeta^{\epsilon - 1}\, d\zeta\}\, d\xi \tag{26}$$

To produce a tractable analytical form of Eq. (26), the term $(1 - \delta\tau)^{\epsilon}$ was expanded for $\delta\tau \to 0$:

$$(1 - \delta\tau)^{\epsilon} \approx 1 - \epsilon\delta\tau + \frac{\epsilon(\epsilon - 1)(\delta\tau)^2}{2} + \ldots \tag{27}$$

For the experiments described in the next section, the largest value of the second-order term in Eq. (27) was less than 0.02, so only the linear term in $\delta\tau$ was kept for the solutions presented below.

For the turbulent boundary-layer flow regime, comparison with Eq. (21) sets $\epsilon = 1/2$. A simple linear extrapolation of T_o analogous to that produced for T_w and P_t [i.e., $T_o = T_o^o + (T_o^f - T_o^o)t/t_f$] produces a linear φ: $\varphi(\xi) = \beta + \chi\xi$. Combining these concepts with Eq. (27) and performing the integrations

in Eq. (26) leads to

$$\theta = \frac{\beta}{\alpha}\left\{\tau^{-1/2} - \frac{1}{2\alpha}\tau^{-1}\left[1-\exp(-2\alpha\tau^{1/2})\right]\right\} + \frac{\chi}{\alpha}\left\{\tau^{1/2} - \frac{3}{2\alpha} + \frac{3}{2\alpha^2}\tau^{-1/2} - \frac{3}{4\alpha^3}\tau^{-1}\left[1-\exp(-2\alpha\tau^{1/2})\right]\right\} + \frac{\beta\delta}{2\alpha}\left\{\left[1+\frac{1}{3}\exp(-2\alpha\tau^{1/2})\right]\tau^{1/2} - \frac{2}{\alpha} + \frac{2}{\alpha^2}\tau^{-1/2} - \frac{1}{\alpha^3}\tau^{-1} \times \left[1-\exp(-2\alpha\tau^{1/2})\right]\right\} \quad (28)$$

where α, β, χ, and δ are dimensionless constants. Their definitions obtained from the discussion above and Eq. (21) are

$$\alpha = c_1\frac{\gamma}{Pr}, \qquad \beta = \frac{\gamma T_o^o}{T_w^o} - 1, \qquad \chi = \frac{\gamma t_a}{T_w^o}\frac{\Delta T_o}{t_f} - 2\frac{t_a}{t_m},$$

$$\delta = \frac{P_f t_a}{(\gamma+1)P^* t_f} \quad (29)$$

If T_o was constant and t_m infinite ($\chi = 0$), and $P^* \gg P_f(\delta\ 0)$, then the basic behavior of Eq. (28) would put $(T_g - T_w)$ proportional to $1/\sqrt{t}$ and independent of $\dot{m}$. Both of these conditions were close to being satisfied for the experiments relevant to this flow regime. In fact, the correction terms [second and third terms of Eq. (28)] amounted to only a few percent of the contribution made by terms on the first line.

For the flow regime with a forced-laminar boundary layer, comparison with Eq. (24) sets $\epsilon = 1/4$, and changes the value of α. To prevent confusion, α has been replaced by $\phi = c_2(\gamma/Pr)\sqrt{\mu/\dot{m}}$ in the solution of Eq. (24) given below. The rest of the above definitions and approximations for β, χ, δ, φ, and τ are still valid, and the approximate form of Eq. (26) is

$$\theta = \frac{\beta}{\phi}\left\{\tau^{-1/4} - \frac{3}{4\phi}\tau^{-1/2} + \frac{3}{8\phi^2}\tau^{-3/4} - \frac{3}{32\phi^3}\tau^{-1}[1-\exp(-4\phi\tau^{1/4})]\right\} + \frac{\chi}{\phi}\left\{\tau^{3/4} - \frac{7}{4\phi}\tau^{1/2} + \frac{21}{8\phi^2}\tau^{1/4} - \frac{105}{32\phi^3} + \frac{105}{32\phi^4}\tau^{-1/4} - \frac{315}{128\phi^5}\tau^{-1/2} + \frac{315}{256\phi^6}\tau^{-3/4} - \frac{315}{1024\phi^7}\tau^{-1}\left[1-\exp(-4\phi\tau^{1/4})\right]\right\} + \frac{\beta\delta}{4\phi}\left\{\tau^{3/4} - \frac{5}{2\phi}\tau^{1/2} + \frac{1}{8\phi^2}\left[33 + \frac{3}{5}\exp(-4\phi\tau^{1/4})\right]\tau^{1/4} - \frac{21}{4\phi^3} + \frac{21}{4\phi^4}\tau^{-1/4} - \frac{63}{16\phi^5}\tau^{-1/2} + \frac{63}{32\phi^6}\tau^{-3/4} - \frac{63}{128\phi^7}\tau^{-1}\left[1-\exp(-4\phi\tau^{1/4})\right]\right\} \quad (30)$$

In this case, if T_o was constant and t_m infinite ($\chi \approx 0$), and $P^* \gg P_f(\delta \approx 0)$, then $(T_g - T_w)$ would be proportional to $\dot{m}^{1/2}$, and $t^{-1/4}$ for $\tau \to \infty$. As before, these conditions were nearly satisfied in the experiments relevant to this flow regime, and the correction terms [second and third terms of Eq. (30)] were not significant.

Experimental Techniques and Procedures

Experiments were conducted in a cylindrical pressure vessel made of structural steel. Table 1 summarizes the mechanical and thermodynamic properties of the tank and the injected gas. The tank was located outside of the laboratory in the open air. Experiments were conducted in the mornings on cloudy winter days when the walls of the tank were at a uniform temperature. The temperature of the vessel walls was monitored by four type J thermocouples in steel sheaths that were taped directly to the vessel outer wall. Experiments were not conducted unless the readings from these four thermocouples were all within 1°C. Two layers of 1-cm-thick rock wool insulation and a waterproof tarpaulin were wrapped around the tank and the four type J thermocouples. Figure 2 shows a schematic of the experimental setup. The insulation ensured a circumferentially uniform wall temperature and an adiabatic outer wall during an experiment.

Temperature measurements in the vessel interior were made with five, bare-wire (AWG-30), type T thermocouples placed in a plane perpendicular to the axis of the cylinder and near the midpoint between the two ends of the vessel (Fig. 2). One of the thermocouples was placed in thermal contact with the wall of the pressure vessel using heat-conducting grease and tape. The other four were held in place by a cross of thin metal tubing. The actual thermocouple junctions were horizontally suspended about 15 cm from the metal cross by the thermocouple wire. The location of these four thermocouples was chosen to detect persistent vertical or horizontal temperature gradients that might have been produced during the fill. Additional thermocouples in the vessel interior were found to be unnecessary because the four thermocouples in the flowing gas displayed the same behavior (see Fig. 3 and discussion below). The five type T thermocouples were hooked to digital electronic thermometers that produced an analog signal (10 mV/°C). These analog voltages were recorded with digital oscilloscopes (LeCroy 9400) or a strip chart recorder (HP7404A).

The response time for the gas temperature measurement system was about 2 or 3 s when the type T thermocouples were exposed to room temperatures and pressures. The response time was much longer when the thermocouples were in near vacuum conditions at the beginning of a run. Because of this, the measurements reported below are not accurate for the first 10–20% of each run. These limitations did not adversely affect this research since the chosen measurement technique was accurate and fast enough to record the portion of the temperature transient that could be predicted by the theoretical model (see assumption 4). In an attempt to fine-tune their internal calibration for the temperature range of interest, the digital electronic thermometers were adjusted so that each one produced the same reading when all five type T thermocouples were placed in a stirred bath of room temperature water. However, this procedure had no effect on the drift of the electronic ice-point references, so the measurement accuracy during the

Table 1 Pressure vessel and injection gas parameters

Vessel properties[a]	
Material	Structural steel (SA 516-70)
Mass	5440 kg
Specific heat capacity	450 J/kg · K
Thermal conductivity	52 W/m · K
Total length	7.3 m
Inner diameter	2.11 m
Wall thickness	1.27 cm
Volume	23.8 m^3
Surface area	50 m^2
Gas properties	
Gas	Argon
Molecular weight	39.948
Density at STP	1.78 kg/m^3
c_p	520 J/kg · K
γ	1.66
R	208 J/kg · K
Thermal conductivity	1.77×10^{-2} W/m · K
Viscosity	2.27×10^{-5} kg/s · m
Joule-Thompson coefficient	3.3×10^{-6} K/Pa

[a]Comments: The inside surface was smooth with a light coat of rust that could not be easily rubbed off, and the outside insulation had an approximate R-factor rating of 3 or 4.

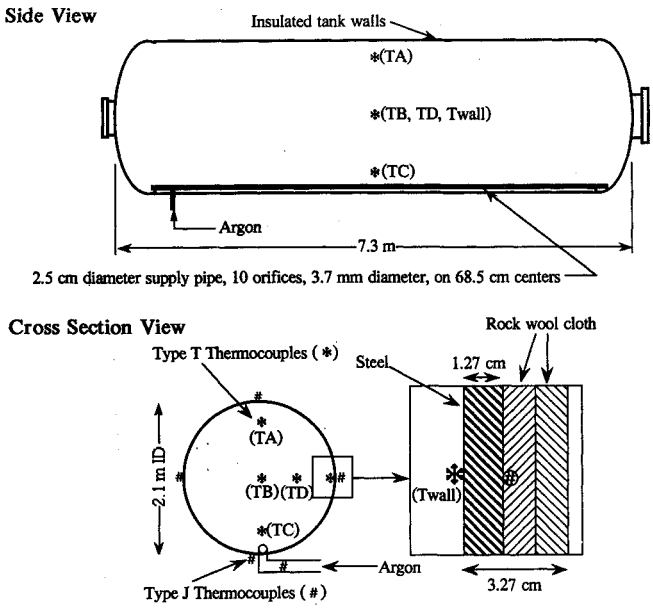

Fig. 2. The experimental setup.

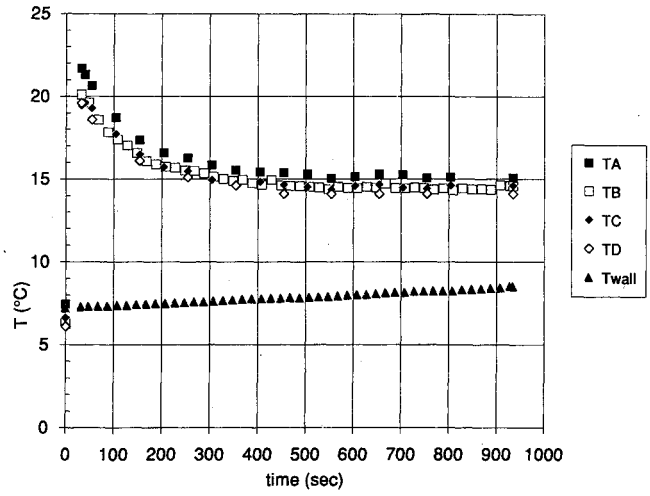

Fig. 3. Typical unreduced temperature data for all five type T thermocouples inside the pressure vessel. TA, TB, TC, TD, and Twall refer to the five type T thermocouples depicted in Fig. 2.

final 80% of a run was believed to be $\pm 1°$ C, with most of this uncertainty due to electronic ice-point drift.

The gas used in the experiments was argon. It was injected at the bottom of the pressure vessel through a 2.5-cm i.d. supply pipe that had ten 3.7-mm-diam. orifices spaced at intervals of 68.5 cm. This orifice spacing of $D/3$ was chosen because it ensured that the jet of injected gas from each orifice would merge with its neighbors before impinging on the far wall of the vessel, and it did not require an unreasonable number of orifices. A type J thermocouple, placed in the supply pipe several centimeters upstream of the first orifice, was used to monitor T_o. The supply pipe was oriented so that the turbulent jets produced by the orifices discharged vertically up and symmetrically impinged on the top inside wall of the pressure vessel. During an experiment, the pressure inside the supply pipe was maintained at a nearly constant value by regulating the flow to it from a high-pressure manifold. The pressure difference between the inside of the supply pipe and the inside of the vessel was usually large enough to ensure sonic conditions at each orifice. Hence, the mass flux was constant to within 1 or 2% because it was determined by the reservoir conditions alone. This is not entirely true for the final portion of the longest run when the orifices unchoked. The pressures in the supply pipe and cylindrical vessel were measured with electronic pressure transducers. The source for the injected gas was a farm of 16 standard high-pressure cylinders manifolded together. These discharged into the supply pipe through a single-stage dome-loaded regulator. The bottle farm was raised to 7.6×10^6 Pa between runs from an argon trailer. The final pressure inside the large cylindrical pressure vessel for most runs was 1.013×10^5 Pa absolute. During a run, the pressure in the bottle farm typically dropped by about 3.4×10^6 Pa.

The experiment was run by evacuating the vessel and then filling it with argon using the injection system described above. The signals from the five type T thermocouples, the type J thermocouple in the supply pipe, and the pressure transducers inside the tank and supply pipe were recorded during the run using the scopes and the chart recorder. Fill times of 40–2000 s were possible with this experimental setup. Longer fill times would have pushed the injection orifices too far from choked conditions and would have required better insulation of the outside of the tank. Shorter fill times would have required increasing the mass flow capacity of the argon delivery plumbing.

About a dozen runs were made. The results were repeatable, and all of the type T thermocouples in the flowing gas displayed the same basic behavior. Figure 3 shows the raw data (some of it digitized by hand from a strip chart record) for all five type T thermocouples during a fill that lasted about 15½ min. The temperature differences shown between the thermocouples in the flowing gas are roughly the same size as the measurement uncertainty. Because this behavior was seen in every run, it was concluded that the mixing action of the injection system did not produce a detectable spatial temperature gradient and that the central thermocouple accurately measured the spatially averaged gas temperature in the vessel. Hence, the data reported in the next section are measured temperature differences between the central and wall thermocouples recorded by the two available digital oscilloscopes. Typical temperature rises in the gas were from 10–40 K. T_w and T_o were usually between 280 and 290 K.

The data reduction involved reading the digitized values of T_g and T_w out of the scope or off of the strip chart record, forming θ, and plotting the results against $\tau = t/t_a$. The approximate Reynolds number of the flow was computed from Eq. (13). For the runs made, the final Reynolds numbers ranged from about 5×10^4 for the longest run (1650 s) to 6×10^5 for the shortest run (44 s).

Results

The results from a run that lasted 128 s are displayed in Fig. 4. The top trace is from the central thermocouple and the lower trace is from the wall thermocouple. The run ended two full divisions beyond the center of the scope screen where the upper curve kinks and the lower curve turns flat. Note that for the entire run the linear extrapolation of the wall temperature is acceptable. The apparent peak in the gas temperature is an artifact of the limited response time of thermocouples in low-density gases. The measurements are believed to accurately track the gas temperature beyond this peak. Figure 5 is a photograph of the strip chart record of the vessel pressure for the same run depicted on Fig. 4. Any deviation from a purely linear increase in vessel pressure was not detected.

Figures 6 and 7, log-log plots of θ versus τ, display the results of the entire experimental investigation. The data points on each figure start at the artificial peak in the measured temperature histories and end at the completion of the fill. Approximately every tenth measurement point is plotted for each run. It should be pointed out that there are only one or two cycles on the vertical axes of these plots; hence, the typical difference between the experimental points and the theoretical predictions, in their range of validity (see discussion below), is only a few percent.

The theoretical curves are calculated from Eqs. (28) and (30) with the visually fitted values of $c_1 = 0.026$ (Fig. 6), and $c_2 = 10.5$ (Fig. 7). Values for the five dimensionless constants (α, β, χ, δ, ϕ) that go into Eqs. (28) and (30) were computed from the measured temperatures and pressures and the information in Table 1. In computing t_a [Eq. (20)] and t_m [Eq. (4)], an adjustment was made to the measured value of T_o for the Joule-Thompson effect that occurred from the pressure drop across the injection orifices.

For fill times less than 100 s (Fig. 6), there is good agreement between the measurements and the fully turbulent theory for the final 80% of a run. Because the Reynolds number increases as the $\sqrt{t}$, the highest Reynolds number data come at the end of the plotted runs. On Fig. 6, note that the highest Reynolds number data from the five runs plotted all fall along the theoretically predicted curve, independent of $\dot{m}$ in accordance with the theory [recall the discussion following Eqs. (21) and (29)]. For fill times in excess of 500 s, there is good agreement between the measurements and the turbulent interior flow/forced-laminar boundary-layer theory for the final 80% of a run. On Fig. 7, the various theoretical curves were generated without modifying the value of c_2 given above. In fact, the vertical spacing of the individual curves with increasing $\dot{m}$ confirms the theoretical approach for this flow regime [recall the discussion following Eqs. (24) and (30)]. The slopes inferred from the measurements on the log-log plots are near the basic theoretical values of $-\frac{1}{2}$ and $-\frac{1}{4}$, underscoring the relatively small contribution of the correction terms.

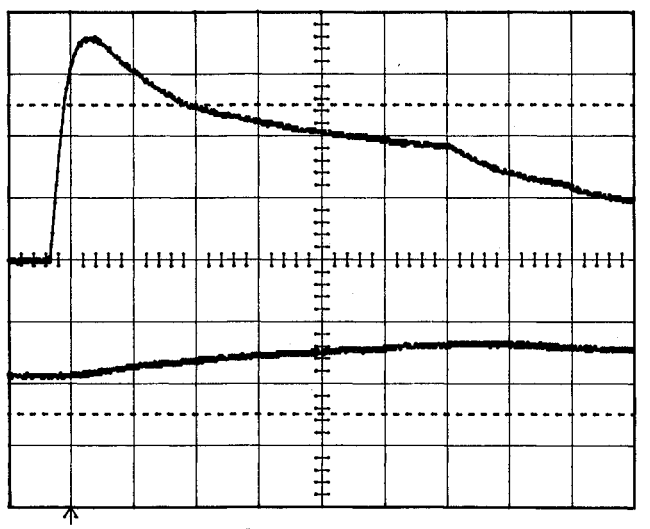

Fig. 4. Oscilloscope traces of gas temperature (top) and vessel wall temperature (bottom) for a run that lasted 128 s. Horizontal scale is 20 s/division. Vertical scale is 10°C/division for the upper trace, and 2°C/division for the lower trace.

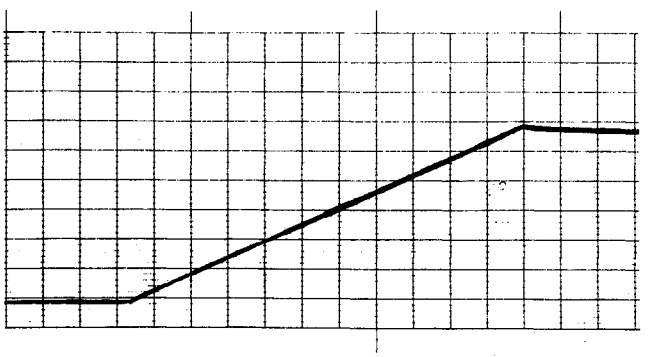

Fig. 5. Strip chart record of the vessel pressure for same run shown on Fig. 4. Horizontal scale is 12 s/division. Vertical scale is 1.72×10^4 Pa/division. The horizontal level on the left before the start of the fill corresponds to vacuum conditions in the pressure vessel.

The greatest disagreement between the experiments and the theory occurs near the beginning of the 62-, 128-, and 134-s fills (Fig. 6) and at the end of the 250-s fill (Fig. 7). The behavior in these regions is likely the result of transition in the boundary layer on the inside of the pressure vessel. A flat-plate, zero pressure gradient boundary layer typically transitions at values of the Reynolds number, based on downstream distance, of about a million.[9] The final Reynolds numbers of the current "transition-range" experiments ($100 \text{ s} < t_f < 500$ s) are about 200,000–400,000. Because a laminar boundary layer that is forced by a turbulent freestream is expected to transition at a lower Reynolds number than a boundary layer driven by a quiescent freestream (see discussion and references in White[9]), the expected and measured Reynolds number ranges of boundary-layer transition appear to overlap. However, wall curvature and pressure gradients along the wall also influence the Reynolds number range in which a boundary layer will transition so that the agreement between these experimental results and those from a flat-plate boundary layer might be mildly fortuitous.

The observed deviation between the measurements and the theory near the end of the 1650-s fill (Fig. 7) is likely the result of the injection orifices unchoking. When the nozzles unchoke, $\dot{m}$ falls, the work input rate drops, and the gas cools faster than the theory predicts. Additionally, an estimate of the global Richardson number for this run indicates that the flow may not be entirely free of the effects of buoyancy.

Discussion

These results can be expanded to spherical vessels filled by a single injection orifice, with thrust J_s and mass flux $\dot{m}_s$, by replacing J and $\dot{m}$ with J_s/D and $\dot{m}_s/D$ in the theoretical

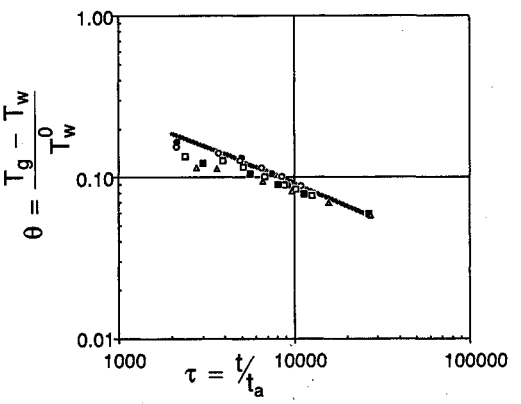

Fig. 6. Normalized mean gas temperature difference θ versus scaled time τ for the fully turbulent flow regime. Legend: fill times, • 44 s, ○ 54 s, □ 62 s, ■ 128 s, △ 134 s, the line is Eq. (28).

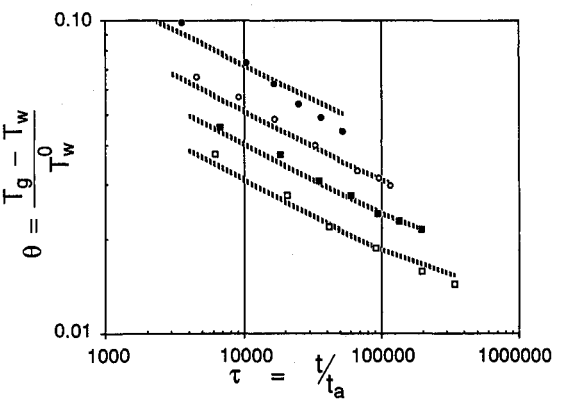

Fig. 7. Normalized mean gas temperature difference θ versus scaled time τ for the turbulent-interior-flow/forced-laminar boundary-layer flow regime. Legend: fill times, • 250 s, ○ 554 s, ■ 934 s, □ 1650 s, the lines are Eq. (30) using the parameters of the corresponding experiments.

development of the second section of this paper. The values of c_1 and c_2 should depend on the vessel geometry also, but the magnitude and flow rate scaling behavior of the temperature transient can be obtained from the same theory for both cylindrical and spherical vessels.

It is also possible to expand the present effort to include pressure vessels that have noninsulated outer walls. This could be implemented by specifying a heat input or removal rate from the wall and then reworking the global energy balance in the second section to achieve the proper form for t_m.

Additionally, the foregoing analysis and results suggest several ways to manipulate the gas temperature inside the pressure vessel during a fill from vacuum. For example, to minimize the temperature difference between the gas and vessel walls, precooled gas with $T_o = T_w/\gamma$ could be injected. Another possibility is tailoring the mass flow rate and inlet temperature so that a given gas temperature (and/or pressure) is reached at a certain time.

Conclusions

The theoretical and experimental efforts previously described lead to several conclusions. First, the basic behavior of the spatially averaged temperature transient in a pressure vessel filled from vacuum and its parametric dependence on the mass flow rate have been correctly documented. Second, the most robust experimental deviations from the theory occur because the wall boundary layer enters transition, a regime that was not treated theoretically. And finally, a detailed model of turbulent heat and momentum transport inside the pressure vessel was not necessary to describe the basic elements of the temperature transient.

Appendix: Temperature Rise of a Calorically Perfect Gas Without Heat Transfer

Consider an ideal throttling process of a calorically perfect gas between two chambers without heat transfer from the gas to the chamber walls. The first chamber, referred to as the supply, is maintained at a constant pressure P_o by a piston. The second chamber, with a fixed volume V_f, referred to as the cavity, is initially evacuated and is connected to the supply by a throttling valve. The throttling process starts when the valve is cracked. Gas flows from the supply to the cavity, and the piston moves to maintain constant pressure in the supply.

The temperature of the gas in the cavity, when the cavity pressure reaches P_f, can be obtained by mass and energy conservation for the slug of gas that ends up in the cavity. The conservation relations are simple in this case.

$$m_g = \rho_o V_o = \rho_f V_f$$

$$E_o + (\text{piston work}) = c_v \rho_o V_o T_o + P_o V_o = E_f = c_v \rho_f V_f T_f$$

Eliminating $P_o V_o$ from the energy equation using $P_o V_o = m_g R T_o$, and dropping the common factor of m_g yields

$$c_v T_o + R T_o = c_v T_f$$

or

$$T_f = \gamma T_o$$

Note that T_f is independent of the final cavity pressure in this case.

Acknowledgments

The authors wish to acknowledge Donald Schultz of Boeing Aerospace for his assistance with the laboratory work. This project was supported by the United States Department of Energy through the Los Alamos National Laboratory under LPCL Contract 9-X28-795R-1.

References

[1]Sutton, G. W., "Effect of Turbulent Fluctuations in a Optically Active Medium," *AIAA Journal,* Vol. 7, No. 9, 1969, pp. 1737–1743.

[2]Yang, H. T., "Formulas for Venting or Charging Gas from a Single Volume," *AIAA Journal,* Vol. 24, No. 10, 1986, pp. 1709–1711.

[3]Kato, H. T., "Comment on: Formulas for Venting or Charging Gas from a Single Volume," *AIAA Journal,* Vol. 25, No. 9, 1987, pp. 1273–1274.

[4]Breidenthal, R. E., Buonadonna, V. R., and Weisbach, M. F., "Mixing Via Jets in Confined Volumes," *Journal of Fluid Mechanics* (to be published).

[5]Ashkenas, H., and Sherman, F. S., "The Structure and Utilization of Supersonic Free Jets in Low-Density Wind Tunnels," *Proceedings of the Fourth Symposium on Rarefied Gas Dynamics,* Academic, New York, Vol. II, 1966, pp. 84–105.

[6]Thompson, P. A., *Compressible-Fluid Dynamics,* McGraw-Hill, New York, 1972, p. 41.

[7]Reynolds, O., "On the Extent and Action of the Heating Surface for Steam Boilers," *Proceedings of the Manchester Literary Philosophic Society,* Vol. 14, 1874, pp. 7–12.

[8]Schlicting, H., *Boundary Layer Theory,* 7th ed., McGraw-Hill, New York, 1960, pp. 298, 707–708.

[9]White, F. M., *Viscous Fluid Flow,* McGraw-Hill, New York, 1974, pp. 433–436, 499.